Organic & Biomolecular Chemistry

Cite this: *Org. Biomol. Chem.*, 2011, **9**, 2751

www.rsc.org/obc

PAPER

Structure and unimolecular chemistry of protonated sulfur betaines, $(CH_3)_2S^+(CH_2)_nCO_2H$ (n = 1 and 2)†‡

Ellie Jung-Hwa Yoo,[a,b,c] Linda Feketeová,[a,b,c] George N. Khairallah,[a,b,c] Jonathan M. White[a,b] and Richard A. J. O'Hair*[a,b,c]

Received 23rd September 2010, Accepted 6th January 2011
DOI: 10.1039/c0ob00770f

The fixed charge zwitterionic sulfur betaines dimethylsulfonioacetate (DMSA) $(CH_3)_2S^+CH_2CO_2^-$ and dimethylsulfoniopropionate (DMSP) $(CH_3)_2S^+(CH_2)_2CO_2^-$ have been synthesized and the structures of their protonated salts $(CH_3)_2S^+CH_2CO_2H\cdots Cl^-$ [DMSA.HCl] and $(CH_3)_2S^+(CH_2)_2CO_2H\cdots Pcr^-$ [DMSP.HPcr] (where Pcr = picrate) have been characterized using X-ray crystallography. The unimolecular chemistry of the $[M+H]^+$ of these betaines was studied using two techniques; collision-induced dissociation (CID) and electron-induced dissociation (EID) in a hybrid linear ion trap Fourier transform ion cyclotron resonance mass spectrometer. Results from the CID study show a richer series of fragmentation reactions for the shorter chain betaine and contrasting main fragmentation pathways. Thus while $(CH_3)_2S^+(CH_2)_2CO_2H$ fragments *via* a neighbouring group reaction to generate $(CH_3)_2S^+H$ and the neutral lactone as the most abundant fragmentation channel, $(CH_3)_2S^+CH_2CO_2H$ fragments *via* a 1,2 elimination reaction to generate $CH_3S^+{=}CH_2$ as the most abundant fragment ion. To gain insights into these fragmentation reactions, DFT calculations were carried out at the B3LYP/6-311++G(2d,p) level of theory. For $(CH_3)_2S^+CH_2CO_2H$, the lowest energy pathway yields $CH_3S^+{=}CH_2$ *via* a six-membered transition state. The two fragment ions observed in CID of $(CH_3)_2S^+(CH_2)_2CO_2H$ are shown to share the same transition state and ion-molecule complex forming either $(CH_3)_2S^+H$ or $(CH_2)_2CO_2H^+$. Finally, EID shows a rich and relatively similar fragmentation channels for both protonated betaines, with radical cleavages being observed, including loss of $^{\bullet}CH_3$.

Introduction

Betaines are fixed charge zwitterions that play key roles in biology.[1] Examples of betaines containing a carboxylate group are shown in Scheme 1. Glycine betaine (GB, **1**), is a biologically important methyl donor in a metabolic pathway linked to the synthesis of neurotransmitters and homocysteine remethylation[2] and also serves as osmoprotectant in many osmotolerant bacteria like lactobacillus acidophilus.[3] The sulfur analogues of GB, dimethylsulfonioacetate (DMSA, **2**) and its higher homologue, dimethylsulfoniopropionate (DMSP, **3**), are produced by a wide variety of photosynthetic organisms including marine algae, phytoplankton, cyanobacteria and/or nearshore halophilic higher plants[4,5] and have been shown to be potential osmoprotectants for many bacteria.[4,6] DMSA is also a potent biological methyl donor,[7] while Seymour and co-workers have recently highlighted the potential influence that phytoplankton-produced DMSP could have on the global climate change.[8]

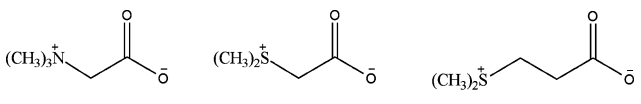

1 **2** **3**

Scheme 1 Examples of fixed charge zwitterionic betaines possessing a carboxylate group: **1**, Glycine betaine (GB); **2**, Dimethylsulfonioacetate (DMSA); **3**, Dimethylsulfoniopropionate (DMSP).

Since amino acids form zwitterions in solution but are in their canonical forms in the gas phase,[9] GB has attracted considerable interest as a model to study the fundamental gas phase chemistry of zwitterions. The presence of the permanent fixed charges can have a profound effect on solvation,[10] cluster chemistry,[11–13] thermochemical properties[14] and unimolecular reactivity.[13,15] For example, Patrick *et al.* measured gas-phase basicity of GB and showed that the permanent charge decreases the proton affinity of the anionic site by over 4 eV in comparison to glycine.[14]

[a]*School of Chemistry, The University of Melbourne, Victoria, 3010, Australia. E-mail: rohair@unimelb.edu.au; Fax: 61 3 9347 5180; Tel: 61 3 8344 2452*
[b]*Bio21 Institute of Molecular Science and Biotechnology, The University of Melbourne, Victoria, 3010, Australia*
[c]*ARC Centre of Excellence for Free Radical Chemistry and Biotechnology, Victoria, 3010, Australia*

† Electronic supplementary information (ESI) available: Cartesian coordinates of all DFT calculated species; Potential energy diagram for all competing reactions calculated relevant to the $[DMSA+H]^+$. CCDC reference numbers 794852 and 794853. For ESI and crystallographic data in CIF or other electronic format see DOI: 10.1039/c0ob00770f

‡ Part 77 of the series "Gas-Phase Ion Chemistry of Biomolecules".

Proton-bound dimers of GB with other molecules form ion-zwitterion structure in which the binding energy depends on the strength of ion-dipole interaction.[11] Electrons can be bound to GB through anion dipole bound state.[16] The important fragmentation pathway of protonated betaine and its neutralized form involved cleavage of the N–C bond between nitrogen and CH_2 of the carboxyl group.[13] The gas phase fragmentation chemistry of protonated betaine clusters are size dependant: while neutral evaporation dominates for the larger clusters,[13] betaine evaporation competes with intracluster S_N2 reactions for the protonated dimer under collision-induced dissociation (CID) conditions.[12c] Electronic excitation of multiply protonated betaine clusters under electron-induced dissociation (EID) conditions can lead to a number of new C–C and C–N bond cleavages, including decarboxylation and CH_3 group transfer.[12e]

Here we: (i) synthesize the sulfur betaines DMSA, **2**, and DMSP, **3**; (ii) provide the first structures of the protonated salts of **2** and **3** *via* X-ray crystallography; (iii) use mass spectrometry and DFT calculations to examine the gas phase unimolecular chemistry of protonated DMSA and DMSP under CID and EID conditions. This approach allows us to evaluate how changing the number of methylene "spacers" between the charge sites influences the structure and gas phase chemistry of sulfur betaines.

Experimental

Materials

All purchased materials were used without further purification: chloroacetic acid 99%, dimethyl sulfide 99%, acrylic acid 99% (Bio Scientific, USA), acetic acid glacial 100% (BDH, AnalaR), methanol (MERCK), picric acid in methanol (MERCK).

Synthesis of DMSA and DMSP

DMSA and DMSP were prepared following the procedures described by Vasudevamurthy *et al.*[17] and Howard *et al.*,[18] respectively. They were characterized by: high resolution mass spectrometry (HRMS) as described below and *via* ^{1}H NMR and ^{13}C NMR spectroscopy carried out on an Inova 400 or Inova 500 spectrometer.

Data for DMSA: HRMS (ESI): $[DMSA+H]^+$ 121.03178 (exptl), 121.03178 (theory). NMR of [DMSA.HCl] salt: ^{1}H NMR (500 MHz, CD_3OD) δ: 5.07 (1H, S), 4.58 (2H,S), 3.06 (6H, S). ^{13}C NMR (125 MHz, CD_3OD) δ: 167.9 (COOH), 47.6(–CH_2–), 26.5 (Me_2S).

Data for DMSP: HRMS (ESI): $[DMSP+H]^+$ 135.04750 (exptl), 135.04743 (theory). NMR of crude DMSP: ^{1}H NMR (500 MHz, CD_3OD) δ: 4.42 (2H, t), 2.71 (2H, t), 2.10 (6H, S). ^{13}C NMR (125 MHz, CD_3OD) δ: 170.3 (COO), 132.2 (–CH_2–), 130.9 (–CH_2–), 18.8 (Me_2S).

X-ray crystallography

DMSA was converted to its hydrochloride salt within 10 days from the mixture of chloroacetic acid and dimethyl sulfide. DMSP was converted to its picrate salt by mixing liquid DMSP with an equivalent amount of picric acid dissolved in a minimum amount of MeOH. Evaporation under reduced pressure afforded crude yellow crystals which were dissolved in a minimum amount of chloroform. Ether diffusion resulted in formation of crystals after 5 days. Intensity data for [DMSP.HPcr] was collected with an Oxford Diffraction Sapphire CCD diffractometer using Cu-Kα radiation (graphite crystal monochromator λ = 1.54184), intensity data for DMSA.HCl was collected with a Bruker SMART Apex CCD detector using Mo-Kα radiation (graphite crystal monochromator $\lambda = 0.71073$). The temperature during data collections was maintained at 130.0(1) K.

Crystal data for [DMSA·HCl]. $C_4H_9ClO_2S$, M = 156.62, T = 130.0(2)K, λ = 0.71073 Å, Monoclinic, space group $P2_1/n$ a = 7.0225(8), $b = 7.3868(8)$ $c = 13.854(1)$ Å, $\beta = 100.912(2)°$. V 705.7(1) Å^3, Z = 4, D_c = 1.474 mg M^{-3} μ(Mo-Kα) 0.752 mm^{-1}, $F(000)$ = 328, crystal size $0.50 \times 0.30 \times 0.15$ mm. 3359 reflections measured, 1608 independent reflections ($R_{int} = 0.0165$) the final R was 0.0269, [$I > 2\sigma(I)$] and $wR(F^2)$ was 0.0768 (all data).

Crystal data for [DMSP·HPcr]. $C_{11}H_{13}N_3O_9S$, M = 363.30, T = 130.0(2)K, λ = 1.54184 Å, Triclinic, space group $P\bar{1}$ a = 7.3627(9), b = 9.5890(9) c = 11.7822(19) Å, α = 69.90(1) β = 73.70(1)° γ = 79.988(9). V 747.0(2) (6) Å^3, $Z = 2$, D_c = 1.615 mg M^{-3} μ(Cu-Kα) 2.469 mm^{-1}, $F(000)$ = 376, crystal size $0.1 \times 0.08 \times 0.01$ mm. 5047 reflections measured, 2860 independent reflections (R_{int} = 0.0636) the final R was 0.0543, [$I > 2\sigma(I)$] and $wR(F^2)$ was 0.1200 (all data).

Mass spectrometry experiments

All experiments were carried out using a hybrid Finnigan LTQ FT (Thermo, Bremen) mass spectrometer equipped with a Finnigan electrospray ionization (ESI) source described in detail previously.[12c,19] The samples were prepared as a 1 mM in 50 : 50 : 1 methanol : water : acetic acid solution, which was introduced into the ESI source of the mass spectrometer at a flow rate of 5.0 µL min^{-1}. Typical ESI conditions used were; spray voltage, 3.0–4.0 kV, capillary temperature, 250 °C, nitrogen sheath gas, 10–30. The capillary voltage and the tube lens offset were tuned to maximize the yield of the desired ion. The injection time was set using the automatic gain control function. The LTQ-FT mass spectrometer consists of: (i) Linear ion Trap (LTQ); (ii) ion transfer optics; and (iii) FT-ICR mass analyzer. For the tandem mass spectrometry experiments, the desired ions produced *via* ESI were trapped in the LTQ and subjected to CID at a He bath gas pressure of *ca* 5×10^{-3} Torr. The CID experiments were performed by mass selecting the desired precursor ion with an activation window of m/z 1–2, and then subjecting it to CID using normalized collision energies between 40%–50% and an activation Q of 0.25 for a period of 30 ms. For high resolution mass analysis and EID, the ions were transferred *via* the ion optics transfer region (~2×10^{-7} Torr) into an FT-ICR cell at a pressure below 1.5×10^{-9} Torr. The FT-ICR cell is supplied with low energy electrons produced by an indirectly heated emitter cathode located downstream of the FT-ICR cell. The energy of electrons is given by the potential difference between the emitter cathode with *ECD offset* of –4.36 V and the grid positioned infront of the cathode, which is variable. Ions were bombarded with electrons of 30 eV energy, *i.e.* corrected 25.6 eV, for 50 ms.

Theoretical calculations

Density functional theory (DFT) calculations were used to examine the structure and the stability of molecules using the Gaussian

03 package.[20] Optimised structures were calculated using the B3-LYP level of theory with 6-311++G(2d,p) basis set for all atoms (C,S,O,H). Transition states for important reaction pathways were connected to the appropriate reactant and product ion minima *via* intrinsic reaction coordinate (IRC) runs. All energies were corrected for zero-point kinetic energies.[21] ($E_{reported} = E_{elctronic} + E_{zpve}$). Vibrational frequency analysis was included to confirm that the structures are local minima or transition states. All calculated structures are available in the ESI.†

Strategies for calculating the global minimum of protonated DMSA and DMSP

In order to calculate the global minima for protonated DMSA and DMSP, and due to the large number of potential structures, we followed a strategy to generate different likely input structures using the Chem3D pro software package.[22] By rotating the main bonds centred around the backbone by 90° and thus changing the corresponding angles, we were able to generate 16 possible input structures for DMSA and 64 for DMSP. Note that this strategy makes no assumption on the conformation of the carboxylic acid group, which generally prefers to be in the *cis* rather than the *trans* form for simple carboxylic acids such as acetic acid.[23] Additionally, we have used the experimentally generated X-ray crystal structures minus the counter anions as input files for optimization. The Initial 16 structures for $[DMSA+H]^+$ were optimised at the HF/3-21G level of theory followed by B3-LYP/6-31G(d). The 7 most stable structures (ESI†) and the X-ray structure were then further optimised, at B3-LYP/6-311++G(2d,p) level of theory.

Similarly, the initial 64 structures found for $[DMSP+H]^+$ were optimised at the same level of theory and the 9 most stable structures as well as the X-ray structure were further optimised at B3-LYP/6-311++G(2d,p) level of theory. The optimization of cation portion of the X-ray structures yielded minima that closely resembled those structures obtained with the aforementioned search as discussed below (also see ESI†).

Results and Discussion

We first compare the X-ray and DFT calculated structures of protonated DMSA and DMSP. The gas phase unimolecular chemistry of protonated DMSA and DMSP are then described using a combination of mass spectrometry experiments and DFT calculations.

Structures of protonated DMSA and DMSP: X-ray *versus* DFT calculations

The thermal ellipsoid plots for [DMSA.HCl] and [DMSP.HPcr] are presented in Fig. 1, while the DFT calculated structures of protonated DMSA and DMSP are given in Fig. 2 and 3. The solid state and DFT calculated gas phase structures are now compared individually.

Protonated DMSA

Seven low lying structures were found for protonated DMSA. The structures were optimized at the B3-LYP/6-311++G(2d,p) level of theory, four of which are shown in Fig. 2. The remaining three rotamers (**5′**, **7′** and **14**) are available in the ESI.† All

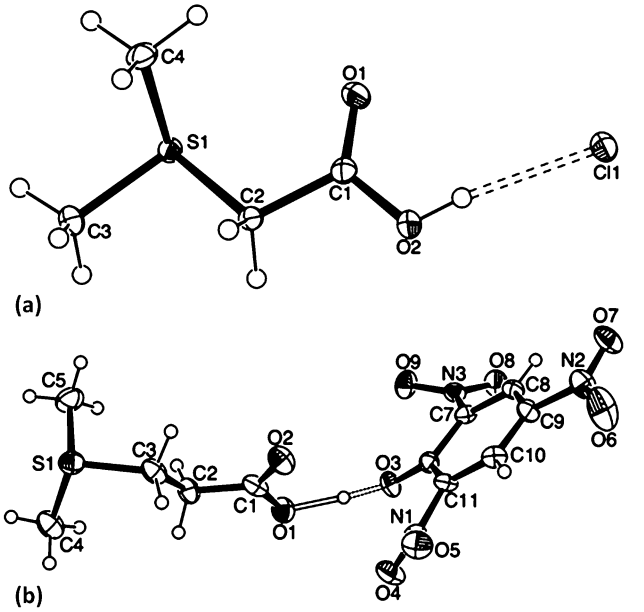

Fig. 1 Thermal ellipsoid plot for: (a) [DMSA·HCl]; (b) [DMSP·HPcr]. Ellipsoids are at the 20% probability level.

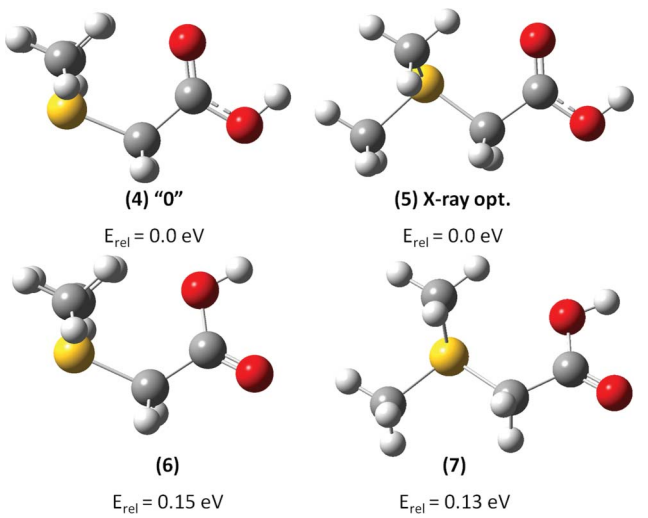

Fig. 2 DFT calculated structures of DMSA, Structure **4** is the global minimum and **5** is the structure resulting from optimization of the isolated cation part of the X-ray salt structure.

structures show carboxyl groups that are in the *cis* form, except for the higher energy conformation **14**, which has its carboxyl group in the *trans* form. Full details (Cartesian coordinates and energies) are available in the ESI (Fig. S1†). The DFT predicted global minimum structure of $[DMSA+H]^+$, found from the conformational search, is shown as **4** in Fig. 2. The S–C–C═O bonds lie in the plane of symmetry. The $(CH_3)_2S$ group and the C═O of the carbonyl have a *syn* arrangement. DFT reoptimization of the $[DMSA+H]^+$ portion of the X-ray structure of the chloride salt (Fig. 1a) gives structure **5**, which has undergone minor structural changes compared to the X-ray structure. **5** is the next lowest energy structure (+0.004 eV), almost isoenergetic with rotamer **4**, found in the conformational search. The comparison between structure **5** and the X-ray structure in bond lengths and

Table 1 Selected structural details of: the DMSA salt; DFT B3-LYP+6-311++G(2d,p) optimised gas phase structure **5** of the isolated cation part of the X-ray salt structure

	X-ray	Opt (**5**)
Bond distance (Å)		
S1–C2	1.794(3)	1.829(4)
S1–C3	1.789(5)	1.818(6)
S1–C4	1.789(7)	1.818(1)
C1–C2	1.507(2)	1.522(9)
C1–O1	1.208(4)	1.201(8)
C1–O2	1.316(2)	1.328(0)
Bond Angles (deg)		
C3–S1–C2	98.9(7)	101.0(2)
C4–S1–C2	103.1(4)	103.6(7)
S1–C2–C1	110.2(6)	108.3(9)
O1–C1–C2	124.0(3)	123.0(3)
O2–C1–C2	110.3(2)	110.4(0)
O1–C1–O2	125.6(5)	126.5(7)
Dihedral Angles		
S1–C2–C1–O1	4.3(2)	8.6(0)
S1–C2–C1–O2	−176.4(6)	−171.9(2)
C3–S1–C2–C1	−178.2(9)	−179.5(3)
C4–S1–C2–C1	−74.4(3)	−73.8(9)

angles is shown in Table 1. One of the CH_3 groups is located in the S–C–C═O plane, while the second CH_3 group is pointing out of the plane, at an angle of 137° with the plane. The other structure (**5′**) shown in the ESI† is isoenergetic with structure **5** and is its mirror image (through the C–S–C–C═O plane). Structure **6** is similar to structure **4** through rotation of the COOH group around the C–C bond, but with a higher relative energy (0.15 eV). Similarly, structure **7** resembles structure **5** with the COOH rotated around the C–C bond and with a relative energy of +0.13 eV.

In the crystal structure, $[DMSA+H]^+$ adopts a conformation which is similar to that for **5** (see Table 1) with a small difference that can be attributed to the chloride counter anion and/or crystal packing forces. The non-bond distance between sulfur and oxygen atom in the crystal structure is 2.888(2) Å, and this distance is within the van der Waals radii (3.32 Å),[24] suggesting that there is an attractive interaction between the sulfur and oxygen atoms that is involved in stabilising this conformation. The natural bond orbital (NBO)[25] calculation reveals that there is no significant interaction between the lone pair of oxygen and the anti-bonding orbital located on the sulfur (For charge and NBO analysis see ESI Fig. S2†). Thus the interaction is mainly electrostatic. In a recent paper, Clark *et al.*[26] have introduced the term σ-hole with reference to Group VII interactions, and Murry *et al.*[27] have reported that this interaction can be extended to Group V and VI. According to the σ-hole bonding concept, the electrostatic interaction in protonated DMSA can be attributed to σ-hole bonding, as the electron-deficient outer lobe of a half-filled *p* bonding orbital of group VI (sulfur) interacts attractively to the nucleophilic site (oxygen).

Protonated DMSP

Fig. 3 shows six low level lying structures found for protonated DMSP at at the B3-LYP/6-311++G(2d,p) level of theory. The remaining three structures are given in the ESI (**8′**, **10′** and **12′**).† Once again, all structures had carboxyl groups which were in the *cis* form (see ESI†). The DFT predicted global minimum structure of $[DMSP+H]^+$, found from the conformational search, is shown as **8** in Fig. 3. Similar to protonated DMSA, the global minimum is involved in an electrostatic interaction arising between the sulfur and oxygen atoms. The non bond distance between sulfur and oxygen atom is 2.893(4) Å, which is within the van der Waals radii, suggesting that there is σ-hole interaction occurring. The mirror image (through C–C–C plane) of structure **8** is given in the ESI.† **9** is the next lowest energy structure (+0.14 eV) found in the conformational search and shows a similar type of stabilization found in structure **4** of $[DMSA+H]^+$, involving hydrogen bonding between the oxygen of the C═O group and the hydrogens of the two methyl groups on the sulfur atom. **10** is lowest lying structure adopting a "zig-zag" conformation (+0.16 eV). DFT reoptimization of the $[DMSP+H]^+$ portion of the X-ray structure of the picrate salt (Fig. 1b) gives structure **11**, which has undergone minor structural changes compared to the X-ray structure. The comparison between structure **11** and the X-ray structure in bond lengths and angles is shown in Table 2. However, the conformation of DMSP in the crystal does not correspond to the calculated global minimum, but rather to a higher energy local minima (see Fig. 3 and Table 2). The adoption of this conformation in the solid state presumably reflects the packing demands associated with the large picrate anion. In contrast to the case of the isoenergetic rotamers **4** and **5** of $[DMSA+H]^+$, **11** is 0.22 eV higher in energy than the global minimum **8**. Structures **12** (+0.26 eV) and **13** (+0.27 eV) both have COOH group that have been rotated around the C–C bond. The "zig-zag" formation is also present in the structure **13**. Since the "zig-zag" structures (**10,13**) are much higher in energies than all other structures of $[DMSP+H]^+$, the interaction between the carbonyl group and the methyl groups on

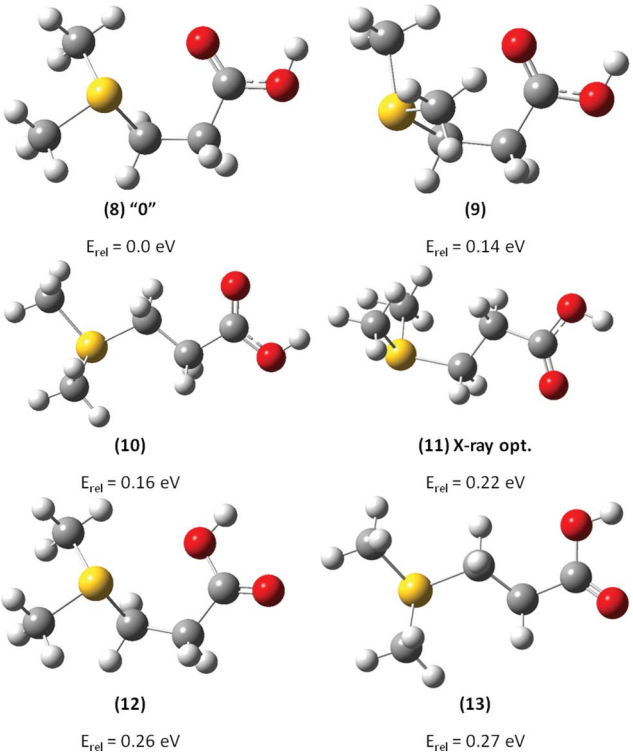

Fig. 3 DFT calculated structures of DMSP, Structure **8** is the global minimum and **11** is the structure resulting from optimization of the isolated cation part of the X-ray salt structure (0.22 eV higher than the global minimum).

Table 2 Selected structural details of: the DMSP salt; DFT B3-LYP+6-311++G(2d,p) optimised gas phase structure **11** of the isolated cation part of the X-ray salt structure

	X-ray	Opt (**11**)
Bond distance (Å)		
S1–C3	1.804(3)	1.834(3)
S1–C4	1.781(0)	1.816(1)
S1–C5	1.780(3)	1.816(3)
C2–C3	1.513(7)	1.521(5)
C1–C2	1.494(9)	1.524(9)
C1–O1	1.327(7)	1.337(8)
C1–O2	1.206(7)	1.201(0)
Bond Angles (deg)		
C3–S1–C4	105.7(5)	105.2(2)
C3–S1–C5	101.8(6)	104.9(9)
S1–C3–C2	116.1(5)	117.5(0)
C1–C2–C3	111.9(4)	108.9(0)
O1–C1–C2	112.0(0)	110.7(3)
O2–C1–C2	124.9(2)	123.9(7)
O1–C1–O2	123.0(6)	125.3(1)
Dihedral Angles		
S1–C3–C2–C1	169.5(5)	178.9(6)
C4–S1–C3–C2	40.1(9)	51.7(1)
C5–S1–C3–C2	–65.6(4)	–56.2(3)
O1–C1–C2–C3	170.2(3)	177.5(2)
O2–C1–C2–C3	–11.4(8)	–2.6(0)

the sulfur most likely plays a role in stabilization of the low energy conformation of $[DMSP+H]^+$.

Gas phase unimolecular chemistry of protonated DMSA

Protonated DMSA, $[DMSA+H]^+$ (*m/z* 121), formed *via* ESI of a solution of DMSA, was mass selected and subjected to low energy CID in the linear ion trap (Fig. 4a) and EID in the FT-ICR cell (Fig. 4b). Eqn (1)–(7) summarize the fragment ions observed and the inferred neutrals formed, but do not detail the mechanism(s) of the fragmentation reactions. An examination of Fig. 4a reveals that the CID spectrum of $[DMSA+H]^+$ is dominated by the formation of the $CH_3S^+{=}CH_2$ fragment ion at *m/z* 61 (eqn (1)), which has been observed earlier in the secondary ion mass spectra of sulfonium ions.[28] The second most abundant fragment ion $(CH_2)_2S^+CH_3$ at *m/z* 75 is likely due to the loss of formic acid (HCO_2H) (eqn (2)). The other minor fragments observed in the CID spectrum are due to loss of H_2O to form $(CH_3)_2S^+$–$CH{=}C{=}O$ ion at *m/z* 103, (eqn (3)); formation of $(CH_3)_2S^+H$ at *m/z* 63, most likely *via* loss of α-lactone (CH_2CO_2) (eqn (4)), and homolytic cleavage leading to the formation of a radical ion $(CH_3)_2S^{\bullet+}$ at *m/z* 62 (eqn (5)). In contrast, the CID spectrum of the analogous protonated nitrogen betaine, $[GB+H]^+$, is much simpler, yielding only two products: $(CH_3)_3N^{\bullet+}$ as the major fragment ion formed *via* homolysis (*cf.* eqn (5)) and the immonium ion $(CH_3)_2N^+{=}CH_2$ (*cf.* eqn (1)).[13]

$$[DMSA+H]^+ \rightarrow CH_3S^+{=}CH_2 + [C_2,H_4,O_2] \quad (1)$$

$$\rightarrow (CH_2)_2S^+CH_3 + HCO_2H \quad (2)$$

$$\rightarrow (CH_3)_2S^+{-}CH{=}C{=}O + H_2O \quad (3)$$

$$\rightarrow (CH_3)_2S^+H + CH_2CO_2 \quad (4)$$

$$\rightarrow (CH_3)_2S^{\bullet+} + {}^{\bullet}CH_2CO_2H \quad (5)$$

$$\rightarrow (CH_3)_2S^+CH_2^{\bullet} + {}^{\bullet}CO_2H \quad (6)$$

$$\rightarrow CH_3S^{\bullet+}CH_2CO_2H + {}^{\bullet}CH_3 \quad (7)$$

Since our experiments do not detect the neutral(s) lost, we turned to DFT calculations to examine the nature of these species. In the case of the major fragment ion $CH_3S^+{=}CH_2$, and as noted in our previous study on protonated GB, there are a number of possible mechanisms that give rise to different losses with an overall stoichiometry of $[C_2,H_4,O_2]$.[13] The mechanims with the lowest barrier (2.02 eV) takes place *via* a six-centred transition state (Fig. 5b, $\mathbf{TS_{4-15}}$) leading to the loss of the enol of acetic acid, $CH_2C(OH)_2$. The products of this reaction are calculated to be higher in energy than their associated transition state suggesting that the product ion-molecule complex undergoes further heating to induce dissociation. This transition state $\mathbf{TS_{4-15}}$ is 0.83 eV and 1.04 eV more favoured than two other transition states found (see ESI†) that could lead respectively to the formation of the same fragment ion through either the loss of $H_2O + CH_2{=}C{=}O$ or loss of acetic acid (ESI Fig. S6†). Thus the favoured mechanism is similair to that found for the formation of $(CH_3)_2N{=}CH_2^+$ from protonated glycine betaine.[13]

The second most abundant fragment ion $(CH_2)_2S^+CH_3$ at *m/z* 75 is due to the loss of formic acid (HCO_2H) (eqn (2)) and most likely posseses a three membered ring structure. Considering the thermochemistry of these products, eqn (2) is found to be the least endothermic (1.03 eV), well below all other fragmentation channels considered (see Fig. 5). However, if $(CH_2)_2S^+CH_3$ does not form a ring structure, but instead froms an open structure (see ESI†), the associated transition state energy ($\mathbf{TS_{4-18}}$) has a barrier of 4.27 eV and is endothermic by 3.8 eV. The energetics for this latter reaction are too high for it to generate an ion of *m/z* 75 as the second most abundant in the low energy CID spectrum. The other minor fragments observed in the CID spectrum are calculated to be due to loss of H_2O to form $(CH_3)_2S^+$–$CH{=}C{=}O$ ion at *m/z* 103, (eqn (3)), loss of α-lactone (CH_2CO_2) forming $(CH_3)_2S^+H$ at *m/z* 63 (eqn (4)), and homolytic cleavage leading to the formation of a radical ion $(CH_3)_2S^{\bullet+}$ at *m/z* 62 (eqn (5)). The potential energy surfaces are shown in Fig. 5. Formation of $(CH_3)_2S^+$–$CH{=}C{=}O$ (eqn (3)) is endothermic by 1.3 eV and has a transition state barrier ($\mathbf{TS_{5'-17}}$) of 2.8 eV, placing it *ca* 0.5 eV higher in energy than the main fragmentation channel. The transition state for the formation of $(CH_3)_2S^+H$ (eqn (4)) ($\mathbf{TS_{14-16}}$) was calculated to be 2.4 eV (> 0.1 eV higher than the main fragmentation channel) and, thermochemically it is endothermic by 2.26 eV. The barrierless homolytic cleavage to form $(CH_3)_2S^{\bullet+}$ was calculated to be 2.78 eV. Further mass spectrometry experiments have proven that the ions observed are due to primary fragmentation channels (data not shown). From these observations, it appears that there exists an interplay between thermodynamics and kinetics in generating the last three least abundant ions.

The EID spectrum shown in Fig. 4b is dominated by fragment ions resulting from radical cleavage reactions leading to the formation of $(CH_3)_2S^{\bullet+}$ (*m/z* 62) (eqn (5)), $(CH_3)_2S^+CH_2^{\bullet}$ (*m/z* 76) (eqn (6)) and $CH_3S^{\bullet+}CH_2CO_2H$ (*m/z* 106) (eqn (7)). The fragment at *m/z* 61 ($CH_3S^+{=}CH_2$), which appeared in the CID spectrum as the most abundant ion, is also observed in the EID spectrum. The EID spectrum of $[DMSA+H]^+$ bears similarities to that of protonated glycine betaine[13] except for one difference: while

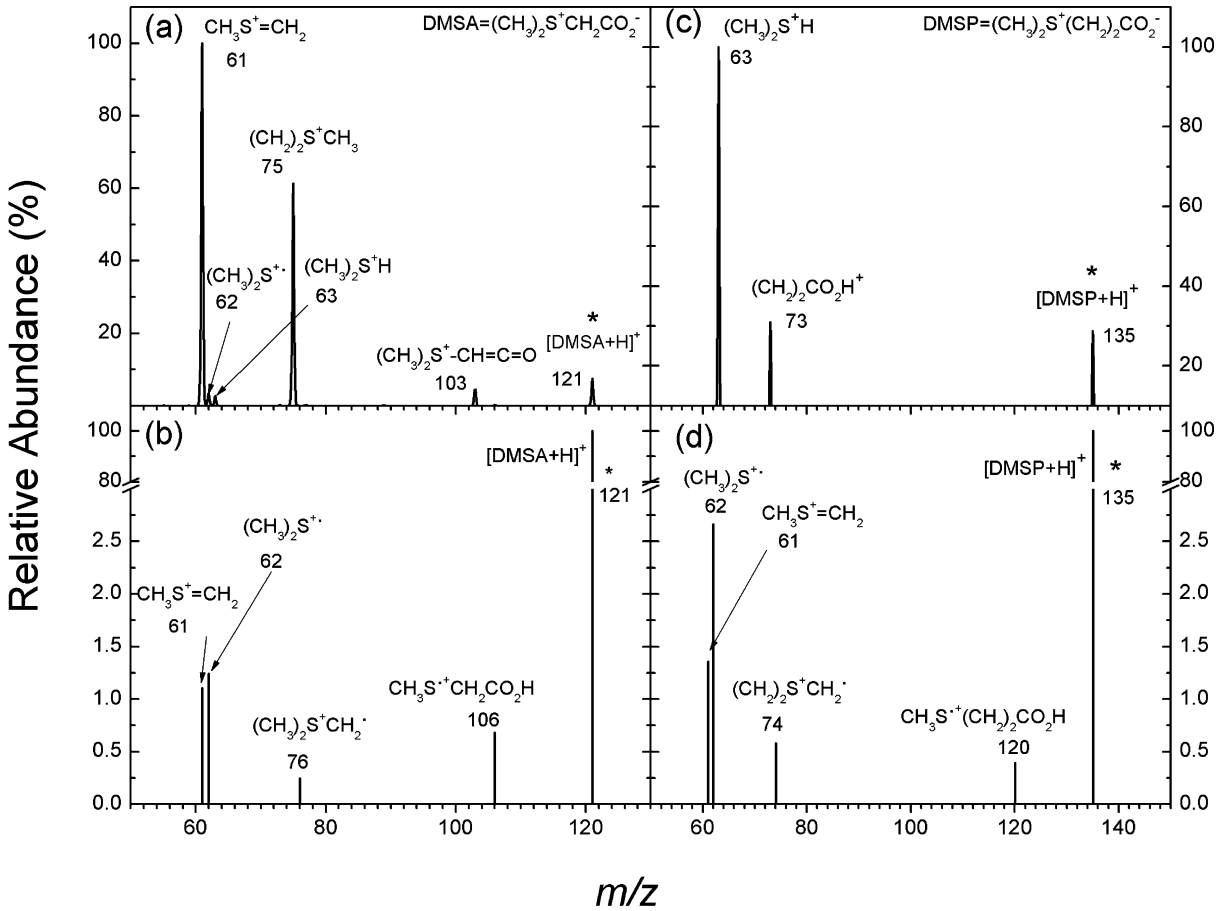

Fig. 4 LTQ-FT MS^2 of sulfur betaines: (a) CID spectrum of $[DMSA+H]^+$ in the linear ion trap (activation time of 30 ms, normalised collision energy 48%); (b) EID spectrum of $[DMSA+H]^+$ in the FT-ICR cell (activation time of 50 ms, corrected electron energy 25.6 eV); (c) CID spectrum of $[DMSP+H]^+$ in the linear ion trap (activation time of 30 ms, normalised collision energy 40%); (d) EID spectrum of $[DMSP+H]^+$ in the FT-ICR cell (activation time of 50 ms, corrected electron energy 25.6 eV).

$[DMSA+H]^+$ loses a neutral radical $^{\bullet}CH_3$, protonated glycine betaine loses CH_4.

Gas phase unimolecular chemistry of protonated DMSP

ESI of a solution of DMSP in methanol generated protonated DMSP, $[DMSP+H]^+$ (*m/z* 121), which was mass selected and subjected to low energy CID in the linear ion trap (Fig. 4c) and EID in the FT-ICR cell (Fig. 4d). Eqn (8)–(13) summarize the fragment ions observed and the inferred neutrals formed, but do not detail the mechanism(s) of the fragmentation reactions. The CID spectrum of $[DMSP+H]^+$ (Fig. 4c) is much simpler than that of $[DMSA+H]^+$ (Fig. 4a), yielding only two fragment ions: $(CH_3)_2S^+H$ at *m/z* 63 *via* loss of $[C_3,H_4,O_2]$ (eqn (8)) and $(CH_2)_2CO_2H^+$ at *m/z* 73, formed *via* the loss of $(CH_3)_2S$ (eqn (9)). Both of these product ions are likely to arise from a neighbouring group reaction[29] in which the carboxylic acid group acts as a nucleophile to displace the $(CH_3)_2S$ leaving group to form an ion-neutral complex (INC)[30] between the protonated lactone and $(CH_3)_2S$. Departure of $(CH_3)_2S$ yields the protonated lactone (eqn (9)) while proton transfer within the INC yields $(CH_3)_2S^+H$ (eqn (8)). Related losses of CH_3SR involving neighbouring group reactions have been reported for alkylated methionine residues[31] and methylated S-methylcysteine, $(CH_3)_2S^+CH_2CH(NH_2)COOH$.[32] In the latter instance, they most likely involve the α-amino group rather than the carboxyl group, as this is expected to be the better neighbouring group.[29]

$$[DMSP+H]^+ \rightarrow (CH_3)_2S^+H + (CH_2)_2CO_2 \quad (8)$$

$$\rightarrow (CH_3)_2S + (CH_2)_2CO_2H^+ \quad (9)$$

$$\rightarrow CH_3S^+{=}CH_2 + (CH_2)_2C(OH)_2 \quad (10)$$

$$\rightarrow (CH_3)_2S^{\bullet+} + {}^{\bullet}(CH_2)_2CO_2H \quad (11)$$

$$\rightarrow (CH_2)_2S^+CH_2^{\bullet} + {}^{\bullet}[C_2,H_5,O_2] \quad (12)$$

$$\rightarrow CH_3S^{\bullet+}(CH_2)_2COOH + {}^{\bullet}CH_3 \quad (13)$$

Calculation shows that these two fragmentation pathways are possible through the same transition state and ion-molecule complex (IMC, **19**) (Fig. 6). In pathway 1, the further dissociation of IMC (**19**) upon heating leads to the formation of the fragment ion $(CH_2)_2CO_2H^+$, this channel was endothermic by 2.12 eV. In pathway 2, IMC (**19**) reorganizes to a different IMC, **20** (we have not calculated the energetic barrier associated with this reorganisation, but it is expected to be small - see ref. 30). The

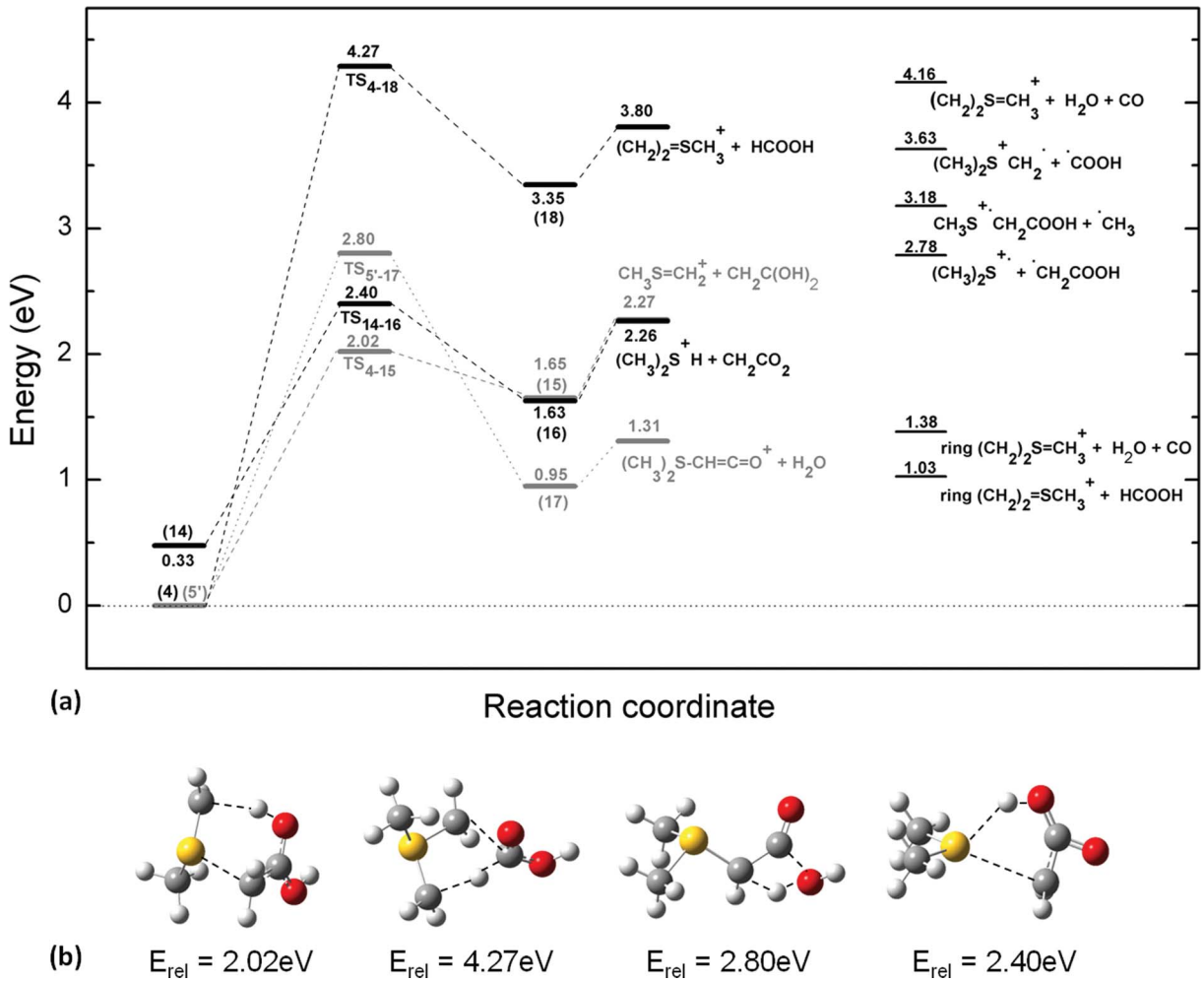

Fig. 5 B3-LYP+6-311++G(2d,p) DFT calculations of the competing reactions shown in eqn (1)–(7) for DMSA. (a) Relative potential energy diagram; (b) optimised geometries of transition states associated with reactions shown in eqn (1), (2), (3) and (4) from left to right.

dissociation of IMC (**20**) leads to $(CH_3)_2S^+H$ *via* a H transfer and loss of $(CH_2)_2CO_2$ (eqn (8)). This channel was endothermic by 1.7 eV. Thus, in the case of DMSP, the DFT calculations are consistent with the experimental observation (Fig. 4c) where the ion at *m*/*z* 63 ($(CH_3)_2S^+H$) was more abundant than $(CH_2)_2CO_2H^+$ at *m*/*z* 73.

EID of $[DMSP+H]^+$ leads to several new fragments in comparison to its CID spectrum, dominated by radical fragment ions. This is not surprising due to the higher energy processes involved. This EID is similar to that of $[DMSA+H]^+$ forming two most abundant ions; at *m*/*z* 61 ($CH_3S^+{=}CH_2$) due to a H transfer from the methyl group (eqn (10)) and the homolytic cleavage product at *m*/*z* 62 ($(CH_3)_2S^{\bullet+}$) (eqn (11)) (*cf.* eqn (1) and 5). The other fragment ions observed include; an ion at *m*/*z* 74 $(CH_2)_2S^+CH_2^{\bullet}$, formed through the loss of $^{\bullet}[C_2,H_5,O_2]$ (eqn (12)), and might likely accommodate a ring structure as determined *via* DFT calculations as being lowest in energy in comparison to other open structures (ESI†). The possible explanation for the loss of $^{\bullet}[C_2,H_5,O_2]$ could be a concerted loss of a radical $^{\bullet}CH_3$ from the parent ion forming the observed fragment ion at *m*/*z* 120 ($CH_3S^{\bullet+}(CH_2)_2CO_2H$) (eqn (13)), this is followed by the H transfer from the second methyl group for the further loss of HCO_2H. The fact that this pathway did not appear in the $[DMSA+H]^+$ case may be due to the longer chain length that gives DMSP more flexibility.

Conclusions

The gas phase low energy CID chemistry of the protonated betaines **1**–**3** depend upon both the cationic site (ammonium (in **1**) *versus* sulfonium (in **2**)) as well as the number of methylene "spacers" between the cationic site and the carboxylic acid group (CH_2 for **2** and CH_2CH_2 for **3**). Whereas CID of $[GB+H]^+$ generates only $(CH_3)_3N^{\bullet+}$ (major) and $(CH_3)_2N^+{=}CH_2$, is observed a much richer CID spectrum for the sulfur analogue $[DMSA+H]^+$ with the following fragment ions occuring: $CH_3S^+CH_2$ (major), $(CH_2)_2S^+CH_3$, $(CH_3)_2S^+CH{=}C{=}O$, $(CH_3)_2S^+H$ and $(CH_3)_2S^{\bullet+}$. In contrast, CID of $[DMSP+H]^+$ generates a simpler spectrum, yielding only $(CH_3)_2S^+H$ (major) and $(CH_2)_2COOH^+$. Both of these ions arise from the same neighbouring group reaction. Thus increasing the number of methylene "spacers" has a profound effect on the unimolecular chemistry of these sulfur betaines, which is directly related to the the size of the lactone rings formed: the α-lactone (CH_2CO_2) formed from $[DMSA+H]^+$ has an activation energy of 2.4 eV ($\mathbf{TS_{14\text{-}16}}$ in Fig. 5b); the β-lactone ($CH_2CH_2CO_2$)

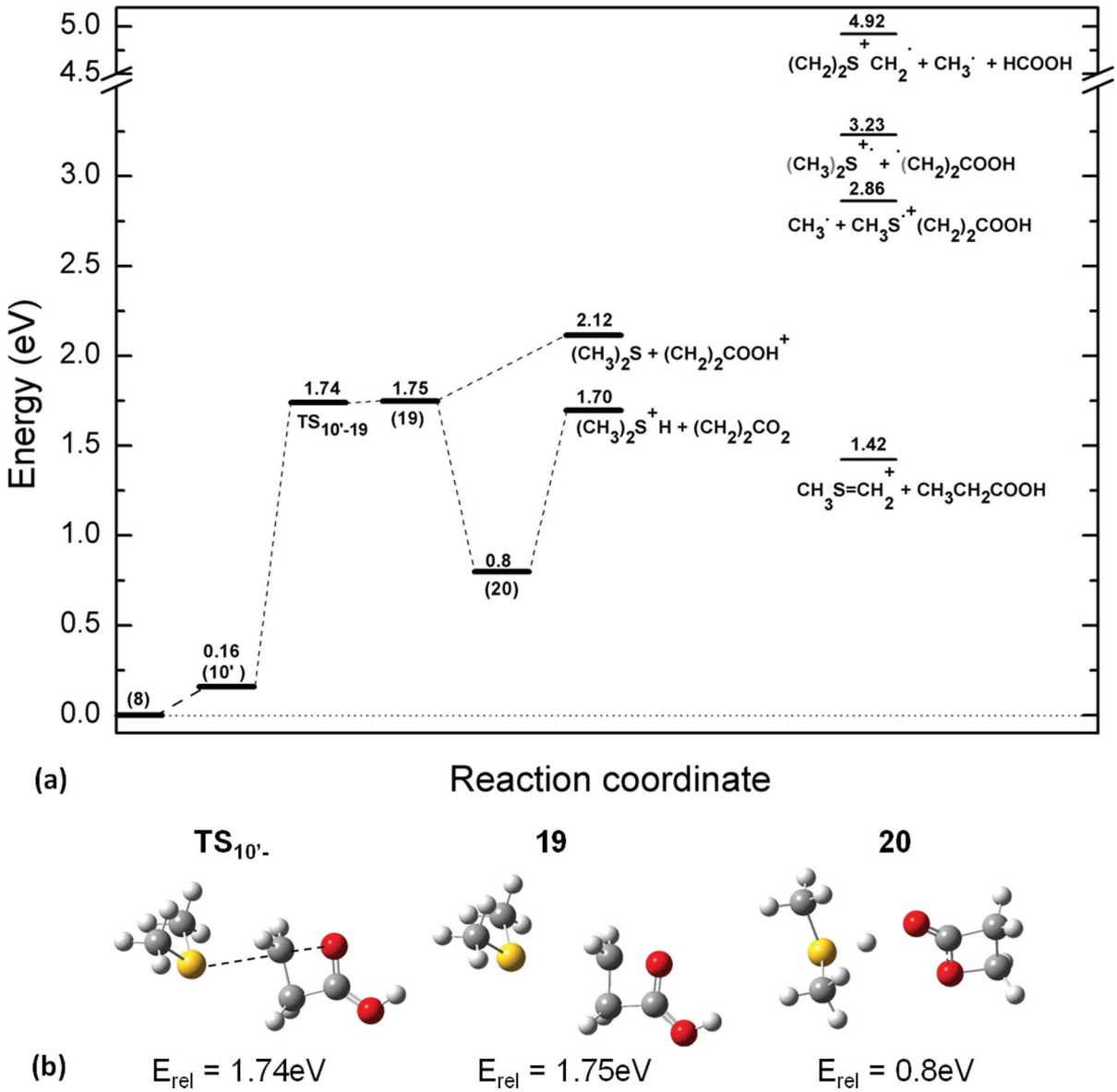

Fig. 6 B3-LYP+6-311++G(2d,p) DFT calculations of the competing reactions shown in eqn (8)–(13) for DMSP. (a) Relative energy diagram in eV; (b) optimised geometries of transition state $\mathbf{TS}_{10'\text{-}19}$ and ion-molecule complexes **19** and **20** associated with reactions shown in eqn (8) and (9).

formed from $[DMSP+H]^+$ has an activation energy of 1.74 eV ($\mathbf{TS}_{10'\text{–}19}$ in Fig. 6b). EID of $[DMSA+H]^+$ and $[DMSP+H]^+$ provides complimentary structural information to CID. Given the role of DMSA as a potent biological methyl donor, future studies will compare the gas phase alkylation reactions of $[DMSA+H]^+$ and $[DMSP+H]^+$.

Acknowledgements

We thank the ARC for financial support *via* the ARC Centre of Excellence for Free Radical Chemistry and Biotechnology. We thank Dr Ina Ritsner-Sambor for discussions on NPA charge analysis. LF and GNK thank the ARC for the award of an APD and an ARF respectively. The authors gratefully acknowledge the generous allocation of computing time from the Victorian Partnership for Advanced Computing (VPAC) Facility. An ARC Lief grant and funding from the Victorian Institute for Chemical Sciences are acknowledged for the purchase of the LTQ-FT mass spectrometer.

Notes and references

1 J. Gorham, in *Amino Acids and their Derivatives in Higher Plants*, ed. R. M. Wallsgrove, Cambridge, 1995, pp. 173–203; T. H. H. Chen and N. Murata, *Curr. Opin. Plant Biol.*, 2002, **5**, 250; S. M. Joyce, A. C. Cassells and S. M. Jain, *Plant Cell, Tissue and Organ Cult.*, 2003, **74**, 103.
2 P. I. Holm, P. M. Ueland, G. Kvalheim and E. A. Lien, *Clin. Chem.*, 2003, **49**, 286.
3 J. B. Jewell and E. R. Kashket, *Appl. Environ. Microbiol.*, 1991, **57**, 2829.
4 A. Cosquer, V. Pichereau, J. A. Pocard, J. Minet, M. Cormier and T. Bernard, *Appl. Environ. Microbio.*, 1999, **65**, 3304 and references therein.
5 G. Jackson and J. Stuckey, *Aquat. Sci.*, 2007, **69**, 419.

6 V. Pichereau, J. A. Pocard, J. Hamelin, C. Blanco and T. Bernard, *Appl. Environ. Microbio.*, 1998, **64**, 1420; A. Baliarda, H. Robert, M. Jebbar, C. Blanco, A. Deschamps and C. Le Marrec, *Int. J. Food Microbiol.*, 2003, **84**, 13; R. P. Kiene, L. P. H. Williams and J. E. Walker, *Aquat. Microb. Ecol.*, 1998, **15**, 39.
7 V. Du Vigneaud, A. W. Moyer and J. P. Chandler, *J. Biol. Chem.*, 1948, **174**, 477.
8 J. R. Seymour, R. Simo, T. Ahmed and R. Stocker, *Science*, 2010, **329**, 342.
9 C. M. Aikens and M. S. Gordon, *J. Am. Chem. Soc.*, 2006, **128**, 12835.
10 R. A. Jockusch, A. S. Lemoff and E. R. Williams, *J. Am. Chem. Soc.*, 2001, **123**, 12255; A. S. Lemoff, M. F. Bush and E. R. Williams, *J. Am. Chem. Soc.*, 2003, **125**, 13576; A. S. Lemoff and E. R. Williams, *J. Am. Soc. Mass Spectrom.*, 2004, **15**, 1014.
11 W. D. Price, R. A. Jockusch and E. R. Williams, *J. Am. Chem. Soc.*, 1998, **120**, 3474.
12 (*a*) D. Ren, M. J. Polce and C. Wesdemiotis, *Int. J. Mass Spectrom.*, 2003, **228**, 933; (*b*) H. A. Cox, R. Hodyss and J. L. Beauchamp, *J. Am. Chem. Soc.*, 2005, **127**, 4084; (*c*) L. Feketeová, G. N. Khairallah and R. A. J. O'Hair, *Eur. J. Mass Spectrom.*, 2008, **14**, 107; (*d*) L. Feketeová and R. A. J. O'Hair, *Chem. Commun.*, 2008, 4942; (*e*) L. Feketeová and R. A. J. O'Hair, *Rapid Commun. Mass Spectrom.*, 2009, **23**, 3259.
13 J. A. Wyer, L. Feketeová, S. B. Nielsen and R. A. J. O'Hair, *Phys. Chem. Chem. Phys.*, 2009, **11**, 8752.
14 J. S. Patrick, S. S. Yang and R. G. Cooks, *J. Am. Chem. Soc.*, 1996, **118**, 231.
15 K. V. Wood, C. C. Bonham, D. Miles, A. P. Rothwell, G. Peel, B. C. Wood and D. Rhodes, *Phytochemistry*, 2002, **59**, 759; P. I. Holm, P. M. Ueland, G. Kvalheim and E. A. Lien, *Clin. Chem.*, 2003, **49**, 286; R. A. J. O'Hair, T. Waters and B. Cao, *Angew. Chem., Int. Ed.*, 2007, **46**, 7048.
16 J. Rak, P. Skurski and M. Gutowski, *J. Chem. Phys.*, 2001, **114**, 10673; W. Zheng, S. Xu, D. Radisic, S. Stokes, X. Li and K. H. Bowen, Jr., *J. Chem. Phys.*, 2005, **122**, 101103.
17 M. Vasudevamurthy, L. Weatherley and M. Lever, *Biocatal. Biotransform.*, 2005, **23**, 285.
18 A. G. Howard and D. W. Russell, *Anal. Chem.*, 1995, **67**, 1293.
19 S. Horning, R. Malek, A. Wieghaus, M. W. Senko, and J. E. P. Syka, Proceedings of the 51st ASMS Conference on Mass Spectrometry and Allied Topics, Montreal, 2003.
20 Gaussian 03, Revision E.01: M. J. Frisch, G. W. Trucks, H. B. Schlegel, G. E. Scuseria, M. A. Robb, J. R. Cheeseman, J. A. Montgomery, Jr., T. Vreven, K. N. Kudin, J. C. Burant, J. M. Millam, S. S. Iyengar, J. Tomasi, V. Barone, B. Mennucci, M. Cossi, G. Scalmani, N. Rega, G. A. Petersson, H. Nakatsuji, M. Hada, M. Ehara, K. Toyota, R. Fukuda, J. Hasegawa, M. Ishida, T. Nakajima, Y. Honda, O. Kitao, H. Nakai, M. Klene, X. Li, J. E. Knox, H. P. Hratchian, J. B. Cross, V. Bakken, C. Adamo, J. Jaramillo, R. Gomperts, R. E. Stratmann, O. Yazyev, A. J. Austin, R. Cammi, C. Pomelli, J. W. Ochterski, P. Y. Ayala, K. Morokuma, G. A. Voth, P. Salvador, J. J. Dannenberg, V. G. Zakrzewski, S. Dapprich, A. D. Daniels, M. C. Strain, O. Farkas, D. K. Malick, A. D. Rabuck, K. Raghavachari, J. B. Foresman, J. V. Ortiz, Q. Cui, A. G. Baboul, S. Clifford, J. Cioslowski, B. B. Stefanov, G. Liu, A. Liashenko, P. Piskorz, I. Komaromi, R. L. Martin, D. J. Fox, T. Keith, M. A. Al-Laham, C. Y. Peng, A. Nanayakkara, M. Challacombe, P. M. W. Gill, B. Johnson, W. Chen, M. W. Wong, C. Gonzalez, and J. A. Pople, Gaussian, Inc., Wallingford CT, 2004.
21 P. Scott and L. Radom, *J. Phys. Chem.*, 1996, **100**, 16502.
22 www.cambridgesoft.com.
23 K. B. Wiberg and K. E. Laidig, *J. Am. Chem. Soc.*, 1987, **109**, 5935.
24 A. Bondi, *J. Phys. Chem.*, 1964, **68**, 441.
25 F. Weinhold and C. R. Landis, *Chem. Educ.: Res. Pract. Eur.*, 2001, **2**, 91.
26 T. Clark, M. Hennemann, J. Murray and P. Politzer, *J. Mol. Model.*, 2007, **13**, 291.
27 J. S. Murray, P. Lane and P. Politzer, *Int. J. Quantum Chem.*, 2008, **108**, 2770.
28 K. L. Duffin and K. L. Busch, *Int. J. Mass Spectrom.*, 1986, **74**, 141.
29 B. Capon and S. P. McManus, in *Neighbouring group participation*, Plenum Press, New York, 1976; R. A. J. O'Hair, *J. Mass Spectrom.*, 2000, **35**, 1377.
30 R. D. Bowen, *Acc. Chem. Res.*, 1991, **24**, 364; R. D. Bowen, *Org. Mass Spectrom.*, 1993, **28**, 1577.
31 R. A. J. O'Hair and G. E. Reid, *Eur. J. Mass Spectrom.*, 1999, **5**, 325; G. E. Reid, K. D. Roberts, R. J. Simpson and R. A. J. O'Hair, *J. Am. Soc. Mass Spectrom.*, 2005, **16**, 1131.
32 G. E. Reid, R. J. Simpson and R. A. J. O'Hair, *J. Am. Soc. Mass Spectrom.*, 2000, **11**, 1047.